



Cite this: *Org. Biomol. Chem.*, 2017, 15, 426

DOI: 10.1039/c6ob02457b

www.rsc.org/obc

Mechanistic insight into the acid-catalyzed isomerization of biomass-derived polysubstituted pyrrolidines: an experimental and DFT study†

Gabriela G. Gerosa, Nicolás Grimblat, Rolando A. Spanevello, Alejandra G. Suárez and Ariel M. Sarotti*

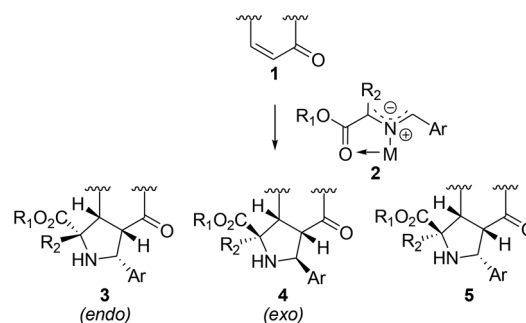
The 1,3-dipolar cycloaddition reactions of azomethine ylides is one of the preferred methods for the synthesis of polysubstituted pyrrolidines. The use of chiral dipolarophiles derived from carbohydrates yields enantiomerically pure pyrrolidines, usually in good to excellent *endo* selectivities, along with other minor stereoisomers. Recently, we found an unusual isomerization event that allowed the isolation of useful pyrrolidines with relative stereochemistries difficult to obtain otherwise. Although a simple and efficient protocol to promote these transformations was developed, the mechanism was not fully unravelled. Herein, after a combination of experimental, spectroscopic and computational studies (using DFT methods) we propose that this isomerization event takes place through a retro-Mannich//Mannich cascade, *via* the formation of an iminium ion with *E* geometry.

Received 10th November 2016,
Accepted 29th November 2016

Introduction

Polysubstituted chiral pyrrolidines are privileged structural motifs in different branches of organic chemistry, present in a wide plethora of natural products.¹ They are also valuable scaffolds in medicinal chemistry, since a wide variety of biologically active compounds share a five-membered nitrogenated heterocyclic ring in their structures.² For example, it has been shown that densely substituted prolines are potent inhibitors of the hepatitis C virus (HCV) polymerase, emerging as promising agents for the treatment of this dreadful disease that affects more than 190 million people all over the world.³ The recent discovery that such molecular architectures can also be effective chiral organocatalysts further increased the interest in their synthesis and chemistry properties.^{4–6}

The 1,3-dipolar cycloaddition reaction between azomethine ylides and α,β -unsaturated carbonyl compounds is a popular and efficient strategy for the stereocontrolled synthesis of pyrrolidines (Scheme 1).⁷ Among several protocols that have been developed for this chemical transformation, the use of stabilized *N*-metalated azomethine ylides (easily obtained *in situ*



Scheme 1 Most common diastereoisomers obtained in the 1,3-dipolar cycloaddition reaction between sugar enones and *N*-metalated azomethine ylides.

upon treatment of α -iminoesters with metal salts in basic media) represents one of the most simple, mild and reliable ones.^{7,8} In order to obtain enantiomerically pure pyrrolidines, this methodology has been extensively studied in its asymmetric variant by using chiral auxiliaries, ligands and catalysts.⁹ Alternatively, the construction of optically active pyrrolidines has also been achieved starting from chiral dipolarophiles, carbohydrates being one of the most promising π -deficient counterparts.^{5,6,10} High levels of facial and regioselectivities have been observed in the 1,3-dipolar cycloaddition between sugar-derived enones and azomethine ylides. Moreover, good to high *endo* selectivities were obtained in these reactions, affording the corresponding *endo* adduct as

Instituto de Química Rosario (CONICET), Facultad de Ciencias Bioquímicas y Farmacéuticas, Universidad Nacional de Rosario, Suipacha 531, Rosario 2000, Argentina. E-mail: sarotti@iquir-conicet.gov.ar

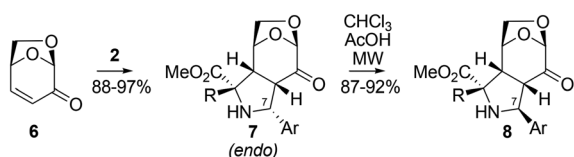
† Electronic supplementary information (ESI) available: Supplementary figures and tables, compound characterization data, copies of ¹H and ¹³C NMR spectra, full reaction coordinate diagrams and Cartesian coordinates of all compounds. See DOI: 10.1039/c6ob02457b

the only isolated isomer, or as the major component in mixtures with other isomeric products that can be obtained in variable yields, depending on the nature of the dipole, dipolarophile and the reaction conditions (Scheme 1).^{5,6,10}

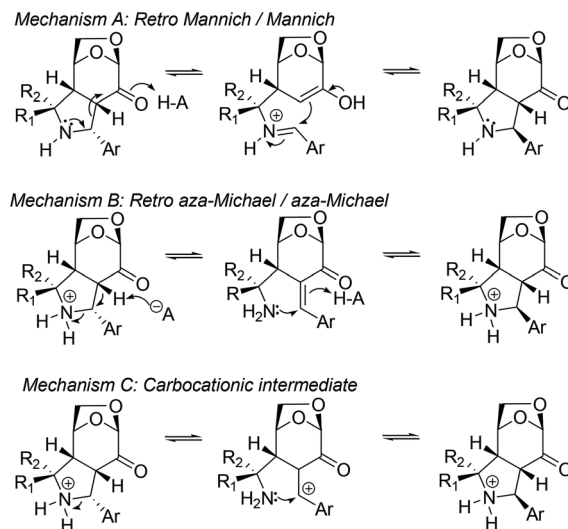
Therefore, unless the *endo* adduct is the synthetic target, the application of these protocols can be limited by not providing flexibility to obtain other stereoisomers in high yields.

Recently, as part of our ongoing interest in the development of valuable chemicals from renewable sources,^{5,6,11} we reported the synthesis of chiral pyrrolidines derived from levoglucosenone in high yields and *endo* selectivities (Scheme 2).⁵ Serendipitously, we observed an epimerization at the benzylic (C-7) position of an *endo* adduct (7) after it had been accidentally left dissolved in CDCl₃ for one month inside the NMR tube. This unexpected and unprecedented isomerization event was further optimized using microwave irradiation, providing a valuable method for the preparation of polysubstituted pyrrolidines with relative stereochemistries difficult to obtain otherwise (8, Scheme 2).⁵ For instance, several precedents can be found in the literature regarding the isolation of stereomutated isomers (such as 5, Scheme 1) that were generally interpreted on the basis of the isomerization of the ylide.^{4,10,12} However, in those studies the aromatic moiety of the dipole and the electron withdrawing group of the dipolarophile are arranged in a *syn* (*endo*) orientation, whereas in our case both groups are *anti*. Interestingly, the isomerized pyrrolidines 8 displayed the highest and most promising organocatalytic activities in asymmetric Diels–Alder reactions among the evaluated isomers, affording the desired products in up to 97% ee.⁶

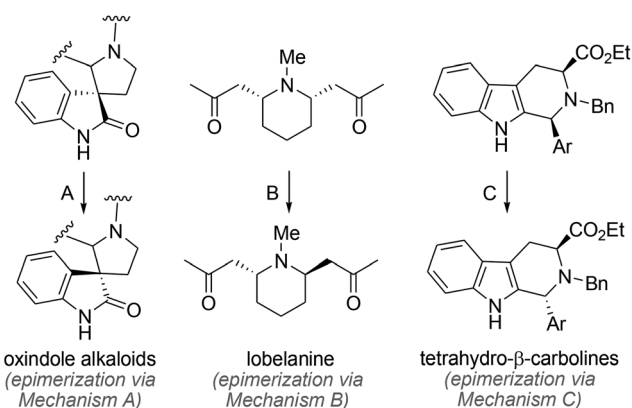
Although we could succeed in developing efficient protocols to promote the transformation of 7 into 8, the mechanism of such transformation could not be fully understood. Preliminary experimental observations allowed us to glimpse and sketch two mechanistic proposals as shown in Scheme 3 (A and B). The first one involves an acid-catalyzed retro-Mannich reaction leading to a resonance-stabilized iminium ion, followed by a Mannich-type closure through the *Si* face of the cation. This path has been proposed to explain the isomerization reactions in spiro oxindole alkaloids (Scheme 4),¹³ and is mechanistically related with the retro-Pictet–Spengler process,¹⁴ considered by the Cook group to account for the *cis/trans* epimerization of tetrahydro- β -carbolines.¹⁵ Moreover, it was quoted by Varela and co-workers to justify the formation of minor isomers in related systems.^{10a} The second mechanistic proposal (mechanism B) consists of a retro-aza-Michael process affording a reactive enone intermediate that following a nucleophilic attack of the



Scheme 2 Synthesis of novel pyrrolidines from levoglucosenone.



Scheme 3 Proposed mechanisms for the isomerization process.



Scheme 4 Three structurally related isomerization reactions that were proposed to occur through the different mechanisms depicted in Scheme 3.

resulting amine through the *Si* face of the β -carbon would lead to the isomerized adduct. Le Bideau, Joseph, and co-workers suggested this path to explain the thermodynamic equilibration of lobelanine, norlobelanine and related analogues (Scheme 4).¹⁶ Finally, though it was not considered by us in our previous study, an additional mechanistic path was possible (mechanism C), involving an heterolytic C–N bond cleavage to produce a benzylic carbocation that could follow a reconnection through the other diastereotopic face to afford the isomerized pyrrolidine. This mechanism was found by Cook to account for the above mentioned *cis/trans* isomerization of substituted tetrahydro- β -carbolines (Scheme 4).¹⁵

Encouraged by the novelty of this isomerization process, along with the promising organocatalytic properties of the isomerized pyrrolidines, we undertook combined experimental, spectroscopic and theoretical studies to unravel the mechanism of such interesting transformations.

Results and discussion

In our previous study, we developed a microwave-assisted methodology to promote the epimerization rapidly and efficiently. However, such reaction conditions were not ideal for mechanistic studies due to the short reaction times and the difficulty in monitoring the progress of the isomerization for kinetic studies. In an effort to develop a new experimental protocol to achieve our goals, we found that gentle heating of a chloroform solution of the corresponding *endo* adduct **7** and a suitable acid at 70 °C afforded the isomerized product **8** in more suitable reaction times. As in the original procedure, total conversion (>99%) was achieved after equilibration for all systems under study, which required 2 to >48 hours depending on the nature of the starting material and the reaction conditions. Next, the effect of the acid strength on the isomerization rate was first analysed using a fixed-time procedure, with **7a** (R = Me, Ar = Ph) as a model compound. After 2 h of heating at 70 °C, the reactions were quenched by the addition of NEt₃, the solvent was evaporated and the crude product was immediately analysed by ¹H NMR. The different chemical shifts exhibited by some diagnostic signals in the starting material (**7a**) and the isomerized product (**8a**) allowed the determination of the isomeric ratio by simple integration of the ¹H NMR spectra of the mixture. Four carboxylic acids with different pK_a values were employed, and the results are shown in Table 1. Acetic acid (the weaker among the studied acids) proved to be ineffective under these reaction conditions since less than 1% of the isomerized product was formed after 2 h of reaction. Significant and systematic increases in the rate were observed using stronger acids, such as chloroacetic acid (entry 2), dichloroacetic acid (entry 3), and trifluoroacetic acid (TFA, entry 4) indicating a clear effect in the acid strength on the isomerization rate. Considering the good performance observed with TFA, and given its usefulness in ¹H NMR experiments (*vide infra*) by not containing additional hydrogen atoms that could interfere in the analysis of the spectra, this was the acid of choice for further studies.

Next, the effect of the concentration of TFA on the epimerization rate was determined. As indicated in Table 2, the epimerization was too low in the absence of acid (entry 1), but significantly increased with the addition of a slight amount of TFA (entry 2), reinforcing our preliminary observation of the need of acidic media to promote such transformations. A modest but systematic increase in the rate was noted using

Table 1 Effect of the acid strength on the isomerization rate^a

Entry	Acid	pK _a	% Isomerization
1	CH ₃ CO ₂ H	4.8	<1%
2	ClCH ₂ CO ₂ H	2.9	37%
3	Cl ₂ CHCO ₂ H	1.3	60%
4	CF ₃ CO ₂ H	0.7	62%

^a All reactions were carried out in chloroform; [7a] = 80 mM; T = 70 °C; 1 equivalent of acid, 2 h.

Table 2 Effect of the acid concentration on the isomerization rate^a

Entry	Eq. TFA	% Isomerization
1	0.0	<1%
2	0.1	53%
3	0.5	57%
4	1.0	62%
5	2.0	40%
6	4.0	30%

^a All reactions were carried out in chloroform; [7a] = 80 mM; T = 70 °C; 2 h.

increasing concentrations of TFA (entries 3 and 4) reaching a maximum at 1 eq. From there, a considerable reduction in the epimerization was observed at higher concentrations of TFA (entries 5 and 6).

We hypothesized that this interesting dependence of the isomerization rate on the concentration of acid could be related to the acid–base equilibrium of the system. In order to have better understanding of this issue, the effect of TFA on the ¹H chemical shifts of **7a** was studied. This approach has been extensively used to understand the protonation of related compounds.¹⁷ Spectra of **7a** in CDCl₃ solution were recorded prior to and after the addition of TFA. Progressive variations in the chemical shifts were observed upon increasing the concentration of the acid, and are shown in Fig. 1. With the addition of 0.5 eq. of TFA, the most affected signals were those assigned to H-7, H-4 and H-3 (in that order), suggesting that the protonation took place mostly on the nitrogen atom, as expected from its higher basicity. The shifting of the other hydrogen atoms was considerably lower, consistent with the higher distance from the interaction site.

The addition of 1.0 eq. of TFA induced a higher deshielding of H-7, H-4 and H-3, suggesting a shift in the equilibrium towards the protonated species. However, under these conditions the shifts of other protons away from the nitrogen atom significantly moved downfield, as was the case of H-1, H-5 and H-6. Upon the addition of higher amounts of TFA the deshielding effect of those signals further increased (Δδ up to 0.28 ppm for H-1, 0.16 ppm for H-5 and 0.33 ppm for H-6),

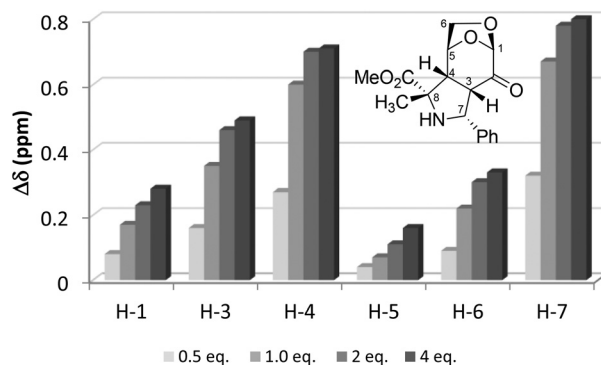
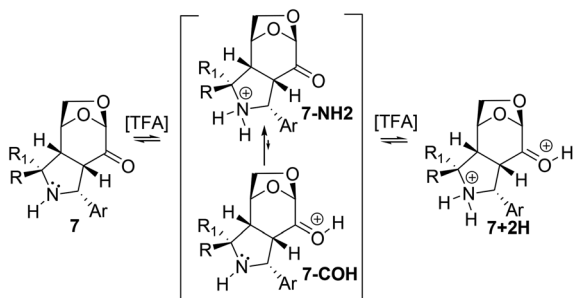


Fig. 1 Changes in the chemical shifts of selected signals of compound **7a** (Δδ = δ_{7a+TFA} - δ_{7a}) upon the addition of increasing amounts of TFA.

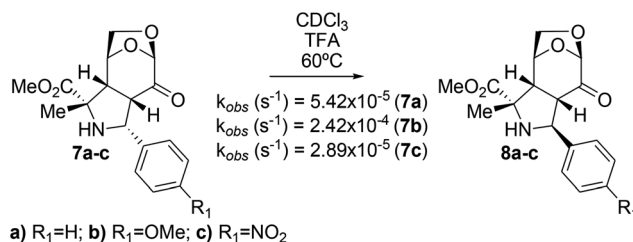
whereas a relatively minor variation in the signals of H-7 and H-4 was noted. These results could be interpreted assuming the formation of di-protonated species by additional protonation of the oxygen atoms (mainly those corresponding to the ketone and 1,6-anhydro groups on the basis of the magnitude of the observed $\Delta\delta$ values).

According to the data herein presented, a simplified acid–base equilibrium depicted in Scheme 5 was proposed, involving a non-protonated species (7), two mono-protonated species, with the protonation at the nitrogen (7-NH2) or the carbonyl oxygen (7-COH), and the di-protonated 7+2H counterpart. The equilibrium should be shifted towards 7 and 7+2H at low and high concentrations of TFA, respectively. On the other hand, the relative proportions of 7-NH2 and its *O*-protonated tautomer (7-COH) might also depend on their relative energies, expecting the former to be the most stable form of the mono-protonated species, prevailing at all ranges of [TFA].

Returning to the rate reduction at high [TFA], and considering the acid–base equilibrium indicated in Scheme 5, we hypothesized that mechanism A (Scheme 3) better fitted the experimental observations. Thus, if the retro-Mannich pathway was involved, a rate reduction would be expected at high concentrations of TFA, as this mechanism would not proceed with the nitrogen protonated. Although the di-protonated and mono-protonated forms are in equilibrium, the concentration of the reactive mono-protonated intermediate (7-COH) would diminish as the concentration of TFA increases. Similar trends were observed by Laus and co-workers in their mechanistic investigation of the isomerization of spiro oxindole alkaloids (Scheme 4),¹³ for which they suggested a retro-Mannich//Mannich cascade. On the other hand, mechanism C should be inconsistent with the reduction of the rate upon the addition of more than 1 eq. of TFA, as a first-order kinetics with respect to the concentration of TFA was observed for the isomerization of trisubstituted-1,2,3,4-tetrahydro- β -carboline operating in a related mechanistic proposal (Scheme 4). Moreover, we explored the isomerization of 7a using TFA-*d* under the same reaction conditions as shown in Table 2, and found a minor kinetic isotopic effect (55% of isomerization with TFA-*d* vs. 62% using TFA), suggesting that the protonation should not be the rate-determining step. In addition, the lack of deuterium incorporation at C-3 provided strong evidence against the retro-aza-Michael path (mechanism B, Scheme 3).



Scheme 5 Proposed acid–base equilibrium.



Scheme 6 Observed rate constants for the isomerizations of 7a–c. [7a–c]₀ = 80 mM; T = 60 °C; [TFA]₀ = 80 mM, CDCl₃.

To gain additional insight into the isomerization process, we studied the dependence of the reaction rate on the electronic nature of the aromatic substituent at the C-7 position. Apart from 7a, we synthesized two isomers bearing strong electron releasing (7b, Ar = 4-OMe-Ph) or withdrawing (7c, Ar = 4-NO₂-Ph) groups at the *para* position of the aromatic ring (Scheme 6).

Interestingly, the isomerization rate (as estimated by the percentage of isomerization observed after 2 h) was strongly sensitive to the electronic effect of the aromatic substituent at C-7. While at 2 h the reaction was completed for compound 7b, 38% of isomerization was observed for 7a, and only 20% in the case of 7c. To have more detailed kinetic information, we next studied the isomerization of 7a–c using ¹H NMR spectroscopy to monitor the progress of the reactions. Thus, pure samples of 7a–c were dissolved in CDCl₃, and the NMR spectra were recorded prior and after the addition of 1 eq. of TFA. In all cases, the final concentration of the corresponding pyrrolidine and TFA was 80 mM. Since the isomerization rate was too slow at room temperature, the NMR probe was heated to 60 °C and maintained at that temperature throughout the experiments, taking the ¹H NMR spectra at regular time intervals. In all cases, the different chemical shifts in the H11 signals exhibited by the starting material (7a–c) and the corresponding isomerized product (8a–c) allowed the determination of the progress of the reaction by integration of those signals in each ¹H NMR spectrum. With the integral values we calculated the concentrations of the starting pyrrolidine (7a–c), and plotted them over time. In all cases, the data nicely fitted to exponential decay functions ($R^2 = 0.9991, 0.9971$ and 0.9996 for 7a, 7b and 7c, respectively), indicating a pseudo-first-order kinetics for the isomerizations. Fig. 2 shows the plot obtained for 7a as a representative example, and the remaining ones are given as part of the ESI.†

The estimated rate constants ($k = 5.42 \times 10^{-5}$, 2.42×10^{-4} and $2.89 \times 10^{-5} \text{ s}^{-1}$ for 7a, 7b and 7c, respectively, Scheme 6) nicely agreed with the reactivity trends discussed above. The negative slope in the Hammett plot strongly suggested the formation of a carbocationic intermediate in direct resonance with the substituent at the *para* position,¹⁸ reinforcing our observations against the aza-Michael mechanism. However, even though all the collected results better fitted with the retro-Mannich path, we could not completely rule out the cationic mechanism proposal.

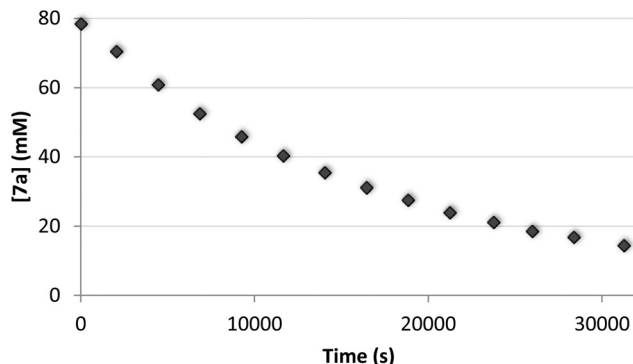


Fig. 2 Concentration vs. time plot obtained for **7a**. $[7a]_0 = 80$ mM; $T = 60$ °C; $[TFA]_0 = 80$ mM, $CDCl_3$.

Detailed analysis of the 1H NMR data collected during the kinetic measurements provided further evidence to solve this issue. In an effort to identify the reactive intermediate that could be formed during the isomerization reactions, we found a very weak signal at ~ 10 ppm (in ratios from 1 : 40 to 1 : 256, relative to the averaged signals of **7** and **8**), as shown in Fig. 3.

The lack of these signals in the 1H NMR spectra of the corresponding samples of **7a–c** recorded before the addition of TFA indicated that the acid should have promoted the formation of this new compound or intermediate. Moreover, we found that the chemical shift of these signals moved downfield when increasing the electron-poor character of the aromatic moiety (9.88 ppm for **7b**, 10.01 ppm for **7a** and 10.16 ppm for **7c**). Initially, we thought that it could be the signal of the $^+N=CH$ proton of an iminium ion that could be formed upon the addition of TFA,¹⁹ but then we realized that it was the signal of the formyl hydrogen of *p*-anisaldehyde (**9b**), benzaldehyde (**9a**), and *p*-nitrobenzaldehyde (**9c**), respectively, showing a perfect match with those recorded from pure analytic samples (9.87 ppm for **9b**, 10.00 for **9a** and 10.16 ppm for **9c**). The formation of **9a**, **9b** and **9c** from **7a**, **7b**, and **7c**, respectively, was thought to proceed *via* the hydrolysis of the corresponding iminium ion **Im** from the low water content present in the system (Scheme 7), representing a key experimental observation in support of mechanism A.

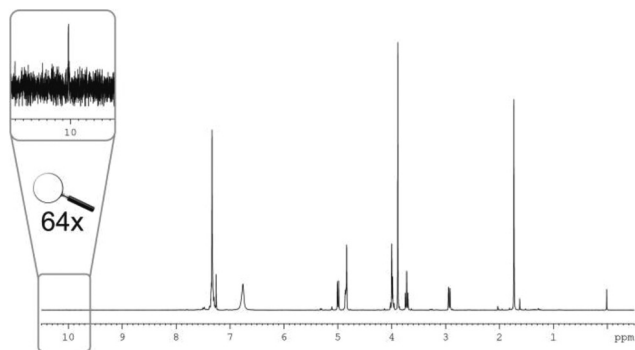
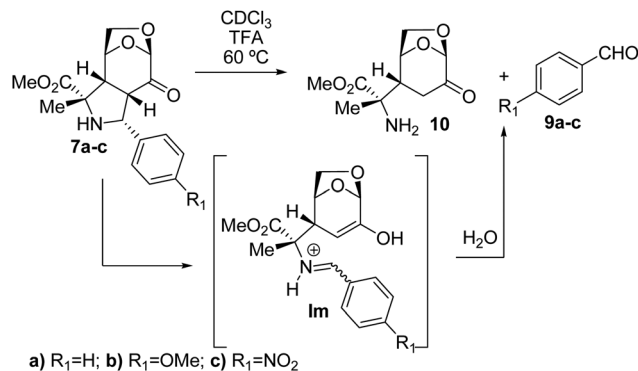


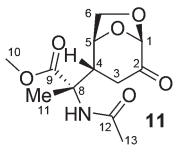
Fig. 3 NMR spectra of **7a** after the addition of 1 eq. of TFA, recorded in $CDCl_3$ at 60 °C.



Scheme 7 Hydrolysis of the iminium ion **Im**, key intermediate in the retro-Mannich/Mannich path.

If this mechanism was correct, then we should have detected compound **10** from the reaction mixtures as well. However, the low amount of hydrolyzed products (as estimated from the intensity of the aldehyde signals) hampered the search in the 1H NMR spectra of the mixtures of **7** and **8** for the signals that could be assigned to **10**, expected in a much more crowded region. We foresaw to run the isomerization reactions by adding increasing amounts of water to facilitate the hydrolysis reactions, though in all cases we obtained the corresponding isomerized pyrrolidine **8a–c** as the major products, even using pure water as solvent. Nevertheless, from these experiments we could isolate a new compound in very low yields (<5%), whose 1H and ^{13}C NMR data were consistent with those expected for **10**. The presence of impurities that could not be eliminated by standard chromatographic procedures complicated the assignment, and this was solved after acetylation of the mixture, isolating the corresponding acetamide **11** in sufficiently pure form to be irrefutably assigned by standard experimental procedures. Thus, the molecular formula $C_{12}H_{17}NO_6$ was deduced from the HRMS ion at m/z 294.09578 [$M + Na$] (calcd 294.09481). IR absorption bands at 1738, 1732 and 1661 cm^{-1} revealed the presence of three carbonyl groups of ketone, ester and amide, respectively, which was confirmed by ^{13}C NMR (199.6 ppm, 172.9 ppm and 170.0 ppm, respectively). Table 3 shows the 1H and ^{13}C data collected for compound **11** that were assigned using COSY, HSQC, HMBC and NOE experiments. The absence of aromatic signals and those corresponding to C-7/H-7 in the starting material, and the presence of a methylene group at C-3, along with the fact that **11** was obtained either from **7a**, **7b** or **7c**, represented key observations to support its structural proposal.

All the experimental evidence discussed above represented strong evidence in favor of the retro-Mannich/Mannich proposal. However, on closer inspection further questions arose regarding the path at which the isomerization reactions took place. As shown in Scheme 8, the configuration at the nitrogen atom in the starting pyrrolidine dictates the geometry of the resulting iminium ion following a retro-Mannich ring opening event. Therefore, the *O*-protonated pyrrolidine with the NH bond directed towards the *endo* face of the molecule

Table 3 ^1H (300 MHz) and ^{13}C (75 MHz) of **11** in CDCl_3


Position	δ_{H} (mult, J , Hz)	δ_{C} (ppm)
1	5.07, s	100.8
2		199.6
3	2.74, dd (17.9, 8.6), 2.62, d (17.9)	32.6
4	3.10, d (8.6)	44.3
5	4.83, bs	73.7
6	4.02–3.97, m	68.7
8		61.5
9		172.9
10	3.74, s	52.9
11	1.66, s	21.0
12		170.0
13	2.01, s	23.5

(7-COH-N) should lead to the *E*-iminium (7-Im-E), whereas the *Z*-iminium (7-Im-Z) might be obtained from the corresponding 7-COH-X pyrrolidine, with the NH bond in the *exo* orientation. Regardless of the initial geometry of the iminium ion, in order to yield the isomerized product, the cyclization must occur through the *Si* face of the electrophile. Therefore, a C8-N single bond rotation should take place to expose the other diastereotopic face of the iminium ion. In principle, it might be expected that the pathway involving the iminium with *E* geometry (*E*-path) should be less energetically demanding. However, there are plenty of studies in recent literature in which the selective formation of *Z*-iminium ions has been postulated.²⁰ Thus, to gain insight into the isomerization event, we undertook DFT calculations at the $\omega\text{B97XD}/6\text{-311+G}^{**}$ level of theory, including chloroform as solvent using SMD,²¹ as implemented in Gaussian 09.²² The ωB97XD functional was developed by Head-Gordon and co-workers,²³ using a version of Grimme's D2 dispersion model, and was successfully employed in recent theoretical studies.²⁴

The paths depicted in Scheme 8 were fully explored for the three systems under study (**7a**, **7b** and **7c**). For simplicity in the presentation, Fig. 4 shows the results obtained with **7a**. Similar trends were observed for the other two compounds under study and are given as part of the ESI.†

According to our calculations, *N*-protonation is the most stable form of the pyrrolidine under acidic media, in perfect agreement with our NMR experiments discussed above.

Regarding the *O*-protonated pyrrolidine, we found that the most stable orientation of the NH bond is *exo*, **7a**-COH-X being 1.6 kcal mol⁻¹ lower in energy than **7a**-COH-N. The corresponding values computed for **7b** and **7c** are 1.4 and 1.9 kcal mol⁻¹, suggesting that the *exo* preference is influenced by the electronic nature of the adjacent aromatic substituent. The computed *exo/endo* ratios at 70 °C are 92 : 8 (**7a**), 88 : 12 (**7b**) and 94 : 6 (**7c**), indicating clear predominance of the corresponding 7-COH-X species in the equilibrium. In contrast, the

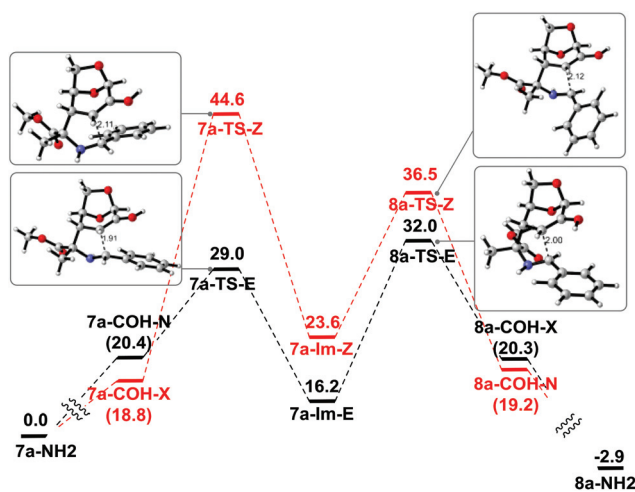
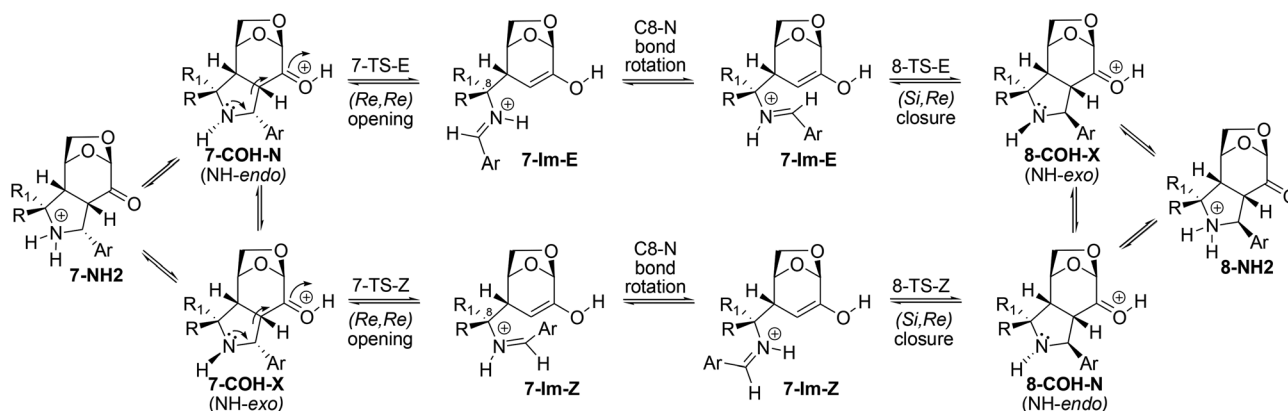


Fig. 4 Full reaction coordinate diagram of the isomerization of **7a** computed at the $\omega\text{B97XD}/6\text{-311+G}^{**}$ level of theory. Relative enthalpies are given in kcal mol⁻¹. Optimized structures and relevant bond-forming and bond-breaking distances are also shown.



Scheme 8 Two different paths for the retro-Mannich//Mannich cascade.

retro-Mannich opening event is much more facilitated from the *endo* counterparts, **7-COH-N**. Thus, the TS that leads to the *E*-iminium (**7a-TS-E**) is 15.6 kcal mol⁻¹ lower in energy than the corresponding **7a-TS-Z**.

The larger barrier computed for the formation of the *Z*-iminium is also well reflected on the relative energies of both geometric isomers. Overall, the formation of **7a-Im-Z** is 7.4 kcal mol⁻¹ more endothermic than **7a-Im-E** ($\Delta H = 23.6$ kcal mol⁻¹ and 16.2 kcal mol⁻¹, respectively). Subsequent ring-closing of Mannich-type is also favored in the *E*-path by 4.5 kcal mol⁻¹ ($\Delta H^\ddagger = 36.5$ kcal mol⁻¹ and 32.0 kcal mol⁻¹ for **8a-TS-Z** and **8a-TS-E**, respectively). As a result, our calculations clearly indicate that the *E*-path should predominate, even though the starting pyrrolidine (**7-COH-N**) is far less stable than the corresponding **7-COH-X** counterpart.

The computational study herein presented also nicely matched the reactivity trend experimentally found for **7a-c**. Fig. 5 shows the preferred path (involving the *E*-iminium) for the three systems under study, with the *O*-protonated species omitted for clarity. A good correlation between the energy barriers and the relative stability of the corresponding iminium ions was observed. The relative ground-state enthalpies of the iminium intermediates closely reflected the influence of the substituent at the aromatic ring ($\Delta H = 13.1$ kcal mol⁻¹, 16.2 kcal mol⁻¹ and 19.9 kcal mol⁻¹ computed for **7b**, **7a** and **7c**, respectively). The effect of the methoxy group to increase the electron density is also responsible for the relative higher stabilization of the incipient iminium ion, resulting in lower barriers of activation. Conversely, the strong electron-withdrawing capacity of the nitro group not only increases the exothermic character of the resulting iminium ion, but also destabilizes the corresponding transition structures ($\Delta H^\ddagger = 29.8$ kcal mol⁻¹ and 28.2 kcal mol⁻¹ for **7c-TS-E** and **7b-TS-E**, respectively, and 33.8 kcal mol⁻¹ and 31.1 kcal mol⁻¹ for **8c-TS-E** and **8b-TS-E**, respectively). The effect of the electronic nature of the substituent at the phenyl ring in the ring-opening and ring-closing Mannich stages can be also seen in

the C3–C7 bond breaking and forming distances, respectively. In general, the more the electron-rich nature of the aromatic ring, the shorter the C3–C7 distances in the transition structures. For instance, the C3–C7 bond lengths in the transition structures for the ring-opening (**TS-1-E**) are 1.91 Å, 1.86 Å and 1.95 Å for **7a**, **7b** and **7c**, respectively, and 2.00 Å, 1.97 Å and 2.01 Å, respectively, for the corresponding ring-closing events (**TS-2-E**).

Moreover, the thermodynamic preference of the isomerized pyrrolidines experimentally found was also nicely reproduced by our calculations. Interestingly, the overall exothermicities computed for **7a**, **7b** and **7c** were 2.9 kcal mol⁻¹, 3.4 kcal mol⁻¹ and 2.2 kcal mol⁻¹, affording the same relative order found for the formation of the iminium ions. Thus, according to these results, the isomerization reactions of electron-rich compounds are benefited both kinetically and thermodynamically.

Conclusions

Experimental, spectroscopic and computational studies provided clear evidence for the acid-promoted isomerization reaction at the benzylic position of chiral pyrrolidines. Three different mechanistic proposals suggested for related systems were taken into consideration, and the experimental evidence indicated that the epimerization takes place through a retro-Mannich//Mannich cascade. DFT calculations at the ω B97XD/6-311+G** level of theory correctly reproduced the experimental findings, and provided further insight suggesting that both the ring-opening and ring-closure steps should occur from a key iminium ion with *E*-configuration.

Experimental section

Experimental methods

All reagents and solvents were used directly as purchased or purified according to standard procedures. Analytical thin layer chromatography was carried out using commercial silica gel plates and visualization was effected with short wavelength UV light (254 nm) and a *p*-anisaldehyde solution (2.5 mL of *p*-anisaldehyde + 2.5 mL of H₂SO₄ + 0.25 mL of AcOH + 95 mL of EtOH) with subsequent heating. Column chromatography was performed with silica gel 60 H, slurry packed, run under a low pressure of nitrogen using mixtures of hexane and ethyl acetate. NMR spectra were recorded at 300 MHz for ¹H, and 75 MHz for ¹³C with CDCl₃ as solvent and (CH₃)₄Si (¹H) or CDCl₃ (¹³C, 76.9 ppm) as internal standards. Chemical shifts are reported in delta (δ) units in parts per million (ppm) and splitting patterns are designated as s, singlet; d, doublet; t, triplet; q, quartet; m, multiplet and br, broad. Coupling constants are recorded in hertz (Hz). Isomeric ratios were determined by ¹H NMR analysis. The structures of the products were determined by a combination of spectroscopic methods such as IR, 1D and 2D NMR (including NOE, DEPT, COSY,

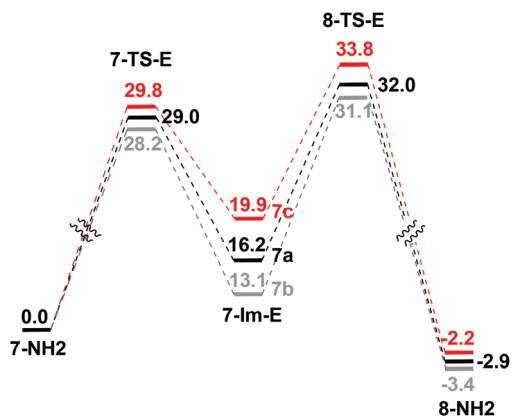


Fig. 5 Reaction coordinate of the preferred path (*E*) computed for **7a** (in black), **7b** (in grey) and **7c** (in red) at the ω B97XD/6-311+G** level of theory. Relative enthalpies are given in kcal mol⁻¹.

HSQC and HMBC experiments) and HRMS. Infrared spectra were recorded using sodium chloride plate pellets. Absorbance frequencies are recorded in reciprocal centimeters (cm^{-1}). High resolution mass spectra (HRMS) were obtained on a TOF-Q LC-MS spectrometer. Optical rotations were determined using a digital polarimeter in 100 mm cells and the sodium D line (589 nm) at room temperature in the solvent and concentration indicated. The melting points are uncorrected. Levoglucosenone (**1**) was prepared from our microwave-assisted pyrolysis of acid-pretreated microcrystalline cellulose.²⁵

General procedure for the synthesis of 7a–c.^{5,6} To a solution of **1** (126 mg, 1 mmol) and the corresponding α -iminoester **11** (1.5 mmol), prepared by condensation of alanine methyl ester hydrochloride and benzaldehyde (**9a**), *p*-anisaldehyde (**9b**), or *p*-nitrobenzaldehyde (**9c**), in dry MeCN (10 mL), were successively added AgOAc (50 mg, 0.3 mmol) and DBU (45 μL , 0.3 mmol). The mixture was stirred for 1 hour at room temperature under an argon atmosphere and in the absence of light (flask covered with aluminum foil). After filtration through Celite, the filtrate was concentrated to dryness under reduced pressure. The crude products were purified by column chromatography with elution with mixtures of hexanes and ethyl acetate to afford pure compounds **7a** (97%), **7b** (86%) and **7c** (63%).

General procedure for the isomerization of 7a–c. The corresponding pyrrolidine **7a–c** (0.1 mmol) was placed in a Hach tube and was dissolved in chloroform (1.25 mL). After the addition of the appropriate amount of acid, the tube was sealed and heated to 70 °C for the corresponding period of time. The reaction was quenched by the addition of NEt_3 , the solvent was evaporated and the crude product was immediately analysed by ^1H NMR. Further purification by column chromatography with elution with mixtures of hexanes and ethyl acetate furnished pure isomerized compounds **8a–c**.

Computational methods

Conformational searches of the reactants, the transition structures (TSS) and the products were run to locate the global minima employing the ωB97XD functional,²³ coupled with the 6-311+G(d,p) basis set. Initially, a large number of geometries were generated using the conformational search module of Hyperchem with the MM+ force field.²⁶ The selected structures were then optimized at the $\omega\text{B97XD}/6\text{-}311\text{+G}^{**}$ level of theory, using Gaussian 09.²² The geometries for all structures were fully optimized in chloroform as solvent using SMD.²¹ The reported thermochemical properties include zero-point energies (ZPEs) without scaling and were calculated at 1 atm, and 343 K. Normal mode analysis was used to confirm the nature of the stationary points and to evaluate the thermochemical properties. All transition structures were confirmed to have only one imaginary frequency corresponding to the formation of the expected bonds. Intrinsic reaction coordinate (IRC) calculations were run to verify the connectivity between the reactants, TSS and products.

Acknowledgements

This research was supported by UNR (BIO 316), ANPCyT (PICT-2012-0970), and CONICET (PIP 11220130100660CO). G. G. G. and N. G. thank CONICET for the award of a fellowship.

References

- (a) J. R. Lewis, *Nat. Prod. Rep.*, 2001, **18**, 95; (b) D. O'Hagan, *Nat. Prod. Rep.*, 2000, **17**, 435.
- (a) P. V. Fish, M. D. Andrews, M. J. Fray, A. Stobie, F. Wakenhut and G. A. Whitlock, *Bioorg. Med. Chem. Lett.*, 2009, **19**, 2829; (b) C. V. Galliford and K. A. Scheidt, *Angew. Chem., Int. Ed.*, 2007, **46**, 8748; (c) F. Bellina and R. Rossi, *Tetrahedron*, 2006, **62**, 7213; (d) M. G. Moloney, P. C. Trippier, M. Yaqoob and Z. Wang, *Curr. Drug Discovery Technol.*, 2004, **1**, 181; (e) S. R. Hussaini and M. G. Moloney, *Org. Biomol. Chem.*, 2003, **1**, 1838; (f) W. H. Pearson, *Pure Appl. Chem.*, 2002, **74**, 1339.
- C. Nájera and J. M. Sansano, *Org. Biomol. Chem.*, 2009, **7**, 4567.
- E. Conde, D. Bello, A. de Cozar, M. Sanchez, M. A. Vazquez and F. P. Cossio, *Chem. Sci.*, 2012, **3**, 1486.
- A. M. Sarotti, R. A. Spanevello, A. G. Suárez, G. A. Echeverría and O. E. Piro, *Org. Lett.*, 2012, **14**, 2556.
- G. G. Gerosa, R. A. Spanevello, A. G. Suárez and A. M. Sarotti, *J. Org. Chem.*, 2015, **80**, 7626.
- (a) L. M. Stanley and M. P. Sibi, *Chem. Rev.*, 2008, **108**, 2887; (b) H. Pellissier, *Tetrahedron*, 2007, **63**, 3235; (c) G. Pandey, P. Banerjee and S. R. Gadre, *Chem. Rev.*, 2006, **106**, 4484; (d) I. Coldham and R. Hufton, *Chem. Rev.*, 2005, **105**, 2765.
- C. Nájera and J. M. Sansano, *Curr. Org. Chem.*, 2003, **7**, 1105.
- (a) C. Nájera and J. M. Sansano, *Angew. Chem., Int. Ed.*, 2005, **44**, 6272; (b) J. Adrio and J. C. Carretero, *Chem. Commun.*, 2011, **47**, 6784; (c) J. Adrio and J. C. Carretero, *Chem. Commun.*, 2014, **50**, 12434.
- (a) G. A. Oliveira Udry, E. Repetto and O. Varela, *J. Org. Chem.*, 2014, **79**, 4992; (b) G. A. Oliveira Udry, E. Repetto, D. R. Vega and O. Varela, *J. Org. Chem.*, 2016, **81**, 4179; (c) G. Bashiardes, C. Cano and B. Mauzé, *Synlett*, 2005, 587.
- (a) M. B. Comba, A. G. Suárez, A. M. Sarotti, M. I. Mangione, R. A. Spanevello and E. D. V. Giordano, *Org. Lett.*, 2016, **18**, 1748; (b) V. Corne, M. C. Botta, E. D. V. Giordano, G. F. Giri, D. F. Llompard, H. D. Biava, A. M. Sarotti, M. I. Mangione, E. G. Mata, A. G. Suárez and R. A. Spanevello, *Pure Appl. Chem.*, 2013, **85**, 1683.
- (a) J. L. García Ruano, A. Tito and M. T. Peromingo, *J. Org. Chem.*, 2002, **67**, 981; (b) J. Casas, R. Grigg, C. Nájera and J. M. Sansano, *Eur. J. Org. Chem.*, 2001, 1971; (c) O. Tsuge, S. Kanemasa and M. Yoshioka, *J. Org. Chem.*, 1988, **53**, 1384.

- 13 (a) E. Wenkert, J. H. Udelhofen and N. K. Bhattacharyya, *J. Am. Chem. Soc.*, 1959, **81**, 3763; (b) G. Cravotto, G. Battista Giovenzana, T. Pilati, M. Sisti and G. Palmisano, *J. Org. Chem.*, 2001, **66**, 8447; (c) G. Laus, D. Brossner, G. Senn and K. Wurst, *J. Chem. Soc., Perkin Trans. 2*, 1996, 1931; (d) G. Laus, *J. Chem. Soc., Perkin Trans. 2*, 1998, 315.
- 14 E. D. Cox and J. M. Cook, *Chem. Rev.*, 1995, **95**, 1797.
- 15 M. L. Van Linn and J. M. Cook, *J. Org. Chem.*, 2010, **75**, 3587.
- 16 Z. Amara, G. Bernadat, P.-E. Venot, P. Retailleau, C. Troufflard, E. Drège, F. Le Bideau and D. Joseph, *Org. Biomol. Chem.*, 2014, **12**, 9797.
- 17 (a) P. Przybylski, K. Pyta, J. Czupryniak, B. Wicher, M. Gdaniec, T. Ossowski and B. Brzezinski, *Org. Biomol. Chem.*, 2010, **8**, 5511; (b) B. Sliter, J. Morgan and A. Greenberg, *J. Org. Chem.*, 2011, **76**, 2770; (c) V. Vimalraj and K. Pandiarajan, *Magn. Reson. Chem.*, 2011, **49**, 682.
- 18 (a) L. P. Hammett, *Chem. Rev.*, 1935, **17**, 125; (b) L. P. Hammett, *J. Am. Chem. Soc.*, 1937, **59**, 96.
- 19 J. E. Johnson, N. M. Morales, A. M. Gorczyca, D. D. Dolliver and M. A. McAllister, *J. Org. Chem.*, 2001, **66**, 7979.
- 20 (a) L. Belding, S. Zaretsky, B. H. Rotstein, A. K. Yudin and T. Duddin, *J. Org. Chem.*, 2014, **79**, 9465; (b) M. H. Haindl, J. Hioe and R. M. Gschwind, *J. Am. Chem. Soc.*, 2015, **137**, 12842; (c) D. Seebach, R. Gilmour, U. Groselj, G. Deniau, C. Sparr, M.-O. Ebert and A. K. Beck, *Helv. Chim. Acta*, 2010, **93**, 603; (d) L. E. Overman and W. C. Trenkle, *Isr. J. Chem.*, 1997, **37**, 23; (e) M. Lukowski, K. Jacobs, P. Hsueh, H. A. Lindsay and M. C. Milletti, *Tetrahedron*, 2009, **65**, 10311.
- 21 A. V. Marenich, C. J. Cramer and D. G. Truhlar, *J. Phys. Chem. B*, 2009, **113**, 6378.
- 22 M. J. Frisch, *et al.*, Gaussian 09, Revision B.01, Gaussian, Inc., Wallingford, CT, 2009.
- 23 J.-D. Chai and M. Head-Gordon, *Phys. Chem. Chem. Phys.*, 2008, **10**, 6615.
- 24 (a) M. Hamzehloueian, Y. Sarrafib and Z. Aghaeib, *RSC Adv.*, 2015, **5**, 76368; (b) L. A. Kondacs, M. V. Pilipecz, Z. Mucsi, B. Balázs, T. Gáti, M. Nyerges, A. Dancsó and P. Nemes, *Eur. J. Org. Chem.*, 2015, 6872; (c) C. Sobhi, A. K. Nacereddine, A. Djerourou, M. Ríos-Gutiérrez and L. R. Domingo, *J. Phys. Org. Chem.*, 2016, DOI: 10.1002/poc.3637, in press.
- 25 A. M. Sarotti, R. A. Spanevello and A. G. Suárez, *Green Chem.*, 2007, **9**, 1139.
- 26 *Hyperchem Professional Release 7.52*, Hypercube, Inc., 2005.